Biotechnology and Bioprocess Engineering 17: 485-499 (2012)
DOI 10.1007/s12257-011-0482-z

RESEARCH PAPER

Effect of the Electrostatic Potential on the Internalization Mechanism of Cell Penetrating Peptides Derived from TIRAP

Karen A. Flores, J. Cristian Salgado, Gerald Zapata-Torres, Ziomara P. Gerdtzen, María-Julieta Gonzalez, and Marcela A. Hermoso

Received: 7 October 2011 / Revised: 4 November 2011 / Accepted: 7 November 2011

Abstract In order to develop future therapeutic applications for cell penetrating peptides (CPPs), it is essential to characterize their internalization mechanisms, as they might affect the stability and the accessibility of the carried drug. Several internalization mechanisms have been described in literature, such as endocytosis and transduction. In this work we study the internalization mechanism in HeLa cells of two TIRAP derived peptides: pepTIRAP and pepTIRAP^{ALA}, where some of the cationic amino acids were replaced with alanines. Detailed analysis of internalization and the peptides electrostatic potential was carried out, to shed light on the internalization mechanism involved. Molecular modeling studies showed that the main difference identified between pepTIRAP and pepTIRAP^{ALA} is the distribution of their electrostatic potential field. The structure of pepTIRAP displays a predominantly positive potential when compared to pepTIRAP^{ALA}, which has a more balanced potential distribution. In addition, docking experiments show that interactions between pepTIRAP and negatively charged molecules on the cellular surface such as heparan sulfate are stronger than the ones exhibited by pepTIRAP^{ALA}. A mathematical model was proposed to quantify the amount of peptide internalized or non-specifically bound to the membrane. The model indicates a stronger interaction of pepTIRAP with the plasma membrane, compared to pepTIRAP^{ALA}. We propose these discrepancies are related to the differences in the electrostatic potential characteristics of each peptide. In the case of pepTIRAP, these interactions lead to the formation of nucleation zones, which are the first stage of the transduction internalization mechanism. These results should be considered for effective design of a cell penetrating peptide.

Keywords: cell penetrating peptide, TIRAP, internalization mechanism, transduction, electrostatic potential

Karen A. Flores, J. Cristian Salgado
Laboratory of Process Modeling and Distributed Computing, Department of Chemical Engineering and Biotechnology, University of Chile, Santiago, Chile

J. Cristian Salgado*, Gerald Zapata-Torres, Ziomara P. Gerdtzen
Millennium Institute for Cell Dynamics and Biotechnology: A Centre for Systems Biology, University of Chile, Santiago, Chile
Tel: +56-2-978-0694; Fax: +56-2-699-1084
E-mail: jsalgado@ing.uchile.cl

Gerald Zapata-Torres
Department of Inorganic and Analytical Chemistry, Faculty of Chemical and Pharmaceutical Sciences, University of Chile, Santiago, Chile

Ziomara P. Gerdtzen
Centre for Biochemical Engineering and Biotechnology, Department of Chemical Engineering and Biotechnology, University of Chile, Santiago, Chile

María-Julieta Gonzalez
Laboratory of Cell Biology, Cell and Molecular Program, Faculty of Medicine, University of Chile, Santiago, Chile

Marcela A. Hermoso*
Laboratory of Innate Immunology, Institute of Biomedical Sciences, Faculty of Medicine, University of Chile, Santiago, Chile
Tel: +56-2-978-6572; Fax: +56-2-978-6979
E-mail: mhermoso@med.uchile.cl

*Both authors share senior authorship

1. Introduction

Cell Penetrating Peptides (CPPs) can internalize and transport molecules that are unable to cross the plasma membrane by themselves, such as drugs [1], peptides [2], proteins [3], peptide nucleic acids (PNAs) [4] and nanoparticles [5]. The CPPs comprise transcription factors

belonging to the family of homodomain proteins such as the *Drosophila melanogaster* Antennapedia (Antp) [6], the TAT protein of HIV-1 [7], fibroblast growth factors 1 and 2 [8], the arginine polymer R9 synthetic peptides [9], among others. The increased therapeutic interest on these peptides focuses in their ability to facilitate the internalization of biologically active molecules [10]. The understanding of the internalization mechanisms used by these peptides contributes to the design of new CPPs with improved characteristics.

There is evidence for several routes of entry used by CPPs, both dependent and independent of the endosomal pathway [11]. The internalization mechanisms for CPPs are not completely understood. Initial evidence suggested the use of a non-endocytosis pathway [12-14]. However, later findings indicate a more significant role of endocytosis as the main internalization pathway [15-17]. The internalization mechanism of CPPs and their cargo *via* endocytosis requires the acidification of the endosome or lysosome followed by the release of CPPs to the cytoplasm. This acidification may chemically alter the transported drug, thereby reducing its biological response [18]. For this reason, it is desirable that CPPs enter directly to the cytoplasm, making it possible for the transported drug to reach its pharmacological target unaltered, therefore eliciting the desired biological response. On the other hand, the transduction mechanism is based on the formation of nucleation zones in restricted areas of the cell membrane, leading to a rapid internalization of CPPs. This mechanism has been described for the internalization of oligo-arginine R9 and TAT peptides in several cell types [19]. Transduction becomes predominant for peptide concentrations above a certain threshold, which depends on cell type and the size of the molecule to be internalized [20].

The efficiency of the biological response of the transported drug strongly relies in the internalization mechanism used. For therapeutic purposes, the challenge is to identify and to characterize the biological response associated with the transported drug and the internalization mechanism used by the CPP. However, it is unclear if CPPs can induce non-specific effects that could interfere the biological action of the transported drug [21].

Proteins in the Toll-like receptor TLR4 signaling pathway are potential targets for therapeutic interventions, where blocking peptides could act as antagonists modulating harmful or chronic inflammatory responses. Several blocking peptides have been designed and used *in vitro* to block the downstream signal transduction pathways of TLR2 and TLR4 [22,23]. TLRs are a key part of the pattern recognition process on the innate immune system [24,25]. They also influence adaptive immunity and affect differentiation of certain immune cell types. TLRs share a cytoplasmic domain or TIR (TLR receptor domain and Interleukin 1, IL-1R), and their activation induces the recruitment of adapter proteins such as MyD88 [26] and TIRAP [27]. A peptide containing the BB loop of TIRAP (highly conserved among TIR proteins) could act as a specific inhibitor of TIRAP, competing for the same interaction site of TLR4 [27]. In fact, a molecule encompassing TIRAP peptide and a CPP based on the Antp domain was used to block the TLR4 signaling pathway [28]. Conflicting results were obtained suggesting that the CPP could interfere with the blocking action of the peptide. This motivates the design of new blocking peptides for the TLR signaling pathway, capable of crossing the plasmatic membrane without the need of CPPs.

It has been reported that transduction is the internalization mechanism used by the arginine oligopeptide R9 and the arginine rich TAT peptide (pepTAT) [19]. The TIRAP peptide (pepTIRAP), which also has a high content of cationic clusters of arginine and lysine residues, internalizes directly into the cytoplasm without altering its structure [29]. This suggests that the presence of these cationic clusters is important for the internalization of these peptides. In fact, it has been reported that when the cationic clusters of pepTIRAP and pepTAT are replaced with alanine residues, the internalization of the resulting peptides (pepTIRAP^{ALA} and pepTAT^{ALA}, respectively) in HeLa and Raw 264.7 cell lines, decreases considerably [29]. This raises the question as to whether peptides with cationic clusters share the same internalization mechanism.

The aim of this work is to contribute to the understanding of the internalization mechanism used by pepTIRAP. To achieve this, three-dimensional models of pepTIRAP, pepTAT and pepTIRAP^{ALA} were developed in order to study their structural and electrostatic potential features. These properties were correlated with experimental internalization results for pepTIRAP and pepTIRAP^{ALA} using a novel mathematical model in order to quantify and explain the internalization of these peptides.

2. Materials and Methods

2.1. Molecular modeling

2.1.1. Modeling of the 3D structures of the peptides

Alignment and selection of structural templates. An exhaustive search of similar sequences for pepTIRAP, pepTIRAP^{ALA} and pepTAT and their alignment was carried out, in order to use them as structural templates. The target peptide sequences are: pepTAT, GRKKRRQRRRPPQ; pepTIRAP, GKMADWFRQTLLKKPKKRPNSPEST and

pepTIRAP^{ALA}, GKMADWFRQTLLAAPAAAPNSPEST. The search was conducted using the online databases: (1) FUGUE (Version 2.0) [30], which uses the HOMSTRAD database [31] and (2) the Protein Data Bank database (PDB) [32]. The templates were selected according to the best values for *Z*-score and *E*-Value for FUGUE and PDB, respectively.

Refinement and validation of the final model. The structures were built using MODELLER [33,34], satisfying the spatial constraints imposed by templates [35,36]. The templates used for comparative modeling of each sequence were (PDB ID): 1JFW, 1K5K, 2W18, 1TAC, 1TVS, 1FW5, 2VCP, 2GRG and 1H8B, for pepTAT; 1SRA, 2DYO and 1H8B, for pepTIRAP and pepTIRAP^{ALA}. The best model was selected from a set of 100 structures generated, according to the lowest DOPE score value. To evaluate the quality of these models, the VADAR online server [37] was used to detect possible structural errors. Upon this, we used MODELLER to correct the errors pointed out by VADAR, generating 100 refinements for each model, and again the best models were selected according to the lowest DOPE score. The addition of hydrogen atoms, capping of the C- and N- amino acid terminals and correction of side chains angles, were carried out using the MolProbity server [38]. The final validation of the structures was performed using VADAR and MolProbity servers.

2.1.2. Calculation of the electrostatic potential field of the peptides

The online server PDB2PQR [39] was used to preprocess the coordinate files generated by MODELLER considering a PARSE force field and pH 7. The calculation of the electrostatic potential field (EPF) for each peptide (pepTAT, pepTIRAP and pepTIRAP^{ALA} was performed using the APBS software [40] as implemented in PyMOL software [41]. This implementation uses FEtk [42,43] to integrate numerically the resulting nonlinear Poisson–Boltzmann equation. The parameters for these calculations were: temperature 310.15 K (37ºC), monovalent ion concentrations of 0.15 M and ionic radius 2.0 Å.

2.1.3. Docking experiments

In order to test the interaction of the pepTIRAP and pepTIRAP^{ALA} with molecules on the cell membrane, docking experiments were performed between these peptides and Heparan Sulfate (HS) molecules. HS glycosaminoglycans are negatively charged, linear polysaccharides composed of repeating disaccharide units. It has been reported that they have a higher percentage of glucuronic acid (GlcA) and N-acetyl-substituted glucosamine (GlcNAc), and a lower percentage of 2-O-sulfo, 6-O-sulfo, and N-sulfo groups [44]. Given that, HS polymers can be represented in docking experiments as a tetrasaccharide composed of two units of GlcA(1-4)GlcNAc and denoted by HS-dp4. The three dimensional structure of HS-dp4 was extracted from its crystal structure (PDB ID code 3E7J). HS-dp4 was optimized and its ESP charges were calculated using Gaussian 98 [45].

Blind and specific dockings experiments were prepared using ADT [46,47] and conducted using the software AutoDock 4.2 [47]. In all experiments, HS-dp4 ligand was considered as flexible and the maximum number of torsions were taken into account in order to explore its conformational space. Peptides (pepTIRAP and pepTIRAP^{ALA}) were considered as rigid. Autodock 4.2 was setup to use a Lamarckian-genetic algorithm to find the best docking conformations, using 5×10^7 evaluation runs. All experiments were repeated 200 times, and the best conformations were analyzed using ADT [46,47] and PyMOL software [41].

2.2. Experimental methods

2.1.1. Culture conditions

For all culture experiments, HeLa cells were seeded in 48-well plates (10^5 cells/well, 40% confluence) and incubated at 37ºC, 5% CO_2 in Dulbecco's modified Eagle's high glucose medium (Gibco, CN 12100046) containing 10% fetal calf serum (Gibco, CN 10091148), 100 U/mL penicillin and 100 μg/mL streptomycin (Gibco, CN 15140122). In order to determine the effect of peptide concentration on viability, cell viability was determined by staining with propidium iodide (PI), an indicator of late apoptosis, using flow cytometry (Becton Dickinson, FACSCalibur model 342976, Serial: E97600098; includes FACStation MACINTOSH G5 PowerMac model A1047, EMC No. 2061).

The threshold of autofluorescence was set to < 0.7%. As a result of cell harvest, *ca.* 10% of the cells are beyond the threshold, *i.e* in late apoptosis.

2.2.2. Peptides

Biotinylated pepTIRAP and pepTIRAP^{ALA} used in this study were kindly provided by Dr. Walter Low. They were produced by solid phase step-wise synthesis (SPSS) using the Fmoc N-terminal protection strategy [29].

2.2.3. Experimental design: Viability

Two control cultures were carried out in order to identify changes in cell distribution when apoptosis is elicited. In the live control curve (LC) cells were treated with PBS. In the apoptotic control curve (AC) cells were treated with Staurosporine, a cell death inductor, in concentrations ranging from 0 to 2 μM.

To study the effect of peptide concentration on viability,

cell were exposed to pepTIRAP and pepTIRAP^{ALA}, solubilized in PBS and dissolved in culture medium, at concentrations ranging from 0 to 100 μM for 16 h. After treatment, cells were harvested using 25 mM EDTA, centrifuged at 1,200 rpm for 5 min at 4ºC, and resuspended in FACS buffer for cytometric analysis.

2.2.4. Experimental design: Internalization

Cells were incubated with pepTIRAP and pepTIRAP^{ALA}, solubilized in PBS and dissolved in culture medium, at 0 and 40 μM for 2 h. Subsequently, cells were harvested with 25 mM EDTA, and cultured in a 96-well plate.

Detection of pepTIRAP and pepTIRAP^{ALA} internalization on HeLa cells using streptavidin-R-PE. The quantification of the internalization of the biotinylated peptides was determined by flow cytometry, using increasing concentrations of streptavidin conjugated to r-phycoerythrin (streptavidin-R-PE) (Molecular Probes, CN S866).

In order to differentiate the fluorescence corresponding to the peptides internalized from the fluorescence associated to peptides linked to the cell surface, one half of the cells, denominated FP cells, were treated with a fixation-permeabilization agent (eBioscience, CN 005523) and the other half with PBS (NFP cells) for 30 min at 4ºC. FP cells were washed with permeabilization buffer 1X and incubated with 0 ~ 100 μg/mL streptavidin-R-PE in permeabilization buffer 1X, for 10 min at room temperature in the dark. NFP cells were washed with PBS and incubated with 0 ~ 100 μg/mL streptavidin-R-PE in PBS, for 10 min at room temperature in the dark. Then, FP cells were washed with permeabilization buffer 1X and resuspended in FACS buffer for flow cytometry analysis. NFP cells were washed with PBS and resuspended in FACS buffer for flow cytometry analysis. In the case of control cells, which were not incubated with peptides, the same procedure described *vide supra* was applied.

Vital cells were gated based on sideward scatter and forward scatter. From this data the mean fluorescence intensity (MFI) was calculated. From the analysis of the experimental fluorescence of vital cells (main population) the heterogeneity of the peptide internalization was characterized based on the event distribution. A mathematical model was proposed and used to discriminate the fluorescence of streptavidin-R-PE associated to: biotinylated peptide internalized and located on the cell membrane, specific binding to biotinylated cytoplasmatic compounds, and non specific associations to the extracellular matrix.

Table 1. Summary of features for the structural models of pepTAT, pepTIRAP, and pepTIRAP^{ALA}

Secondary structure	pepTAT	pepTIRAP	pepTIRAP^{ALA}
α-helix	9[a] (69%)[b]	19 (76%)	22 (88%)
β-sheet	0 (0%)	0 (0%)	0 (0%)
Coil	4 (31%)	6 (24%)	3 (12%)

[a]Number of residues in each type of secondary structure and [b]their respective percentage.

3. Results and Discussion

3.1. Structural analysis of the 3D models for pepTIRAP, pepTIRAP^{ALA}, and pepTAT

The structural models obtained have high structural similarities among them (Table 1), with a predominantly α-helical secondary structure that involves more than 69% of the amino acids in all models. Notice in Fig. 1, that the replacement of lysine (Lys, K) and arginine (Arg, R) in pepTIRAP with alanine (Ala, A) has a little impact in the three-dimensional structure of the peptide. In fact, the root mean square deviation (RMSD) between the structures of pepTIRAP and pepTIRAP^{ALA} is 0.639 Å, and the α-helix percentage increases only from 76 to 88% with respect to pepTIRAP.

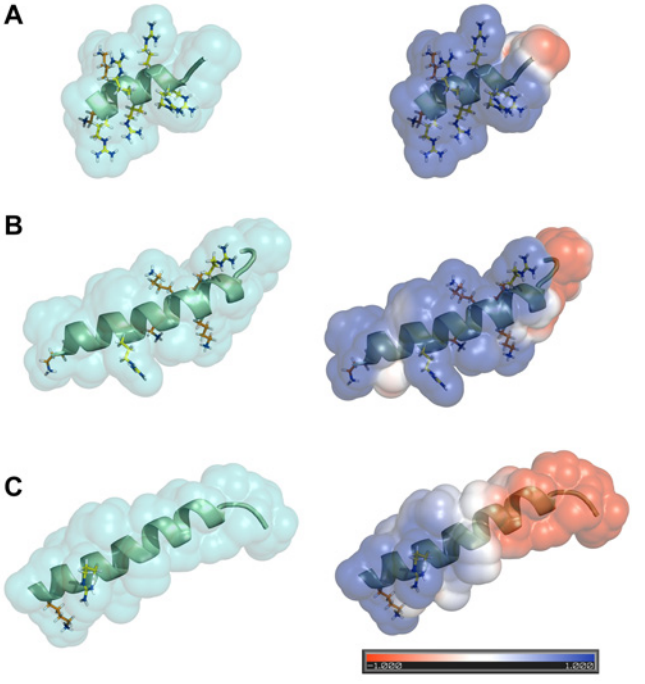

Fig. 1. Structural models and their electrostatic potential on the surface for (A) pepTAT, (B) pepTIRAP, and (C) pepTIRAP^{ALA}. The structural models obtained by using MODELLER are on the left. The electrostatic potential on the surface of the peptides are shown on the right. Positive potential is colored blue, while negative potential is colored red. The cationic amino acids of the peptides are displayed using stick representation. In this figure it can be noticed a more predominant positive EPF on the surface of both pepTAT and pepTIRAP. The pepTIRAP^{ALA} structure displays a more evenly distributed EPF. Images were prepared using PyMol [41].

MolProbity and VADAR servers were used to evaluate the models. In general, all models exhibit evaluation metrics in the acceptable range, except for a few cases detailed below. The number of Ramachandran outliers in the final models for pepTIRAP, pepTIRAP^{ALA} and pepTAT is zero, therefore there are no residues with poorly defined bonds and angles to be found. For the pepTIRAP model, the fractional volume of all amino acids are in the acceptable range, with the exception of residue 6 which has a border line value of 0.78. These results indicate that the model is efficiently packed. A fractional accessible surface area of 1.16 was obtained for residue 25 in pepTIRAP^{ALA}, but this deviation could be due to the fact that this residue is located at the end of the peptide. Based on all of these information, the models are considered acceptable for further studies.

3.2. Electrostatic potential for pepTIRAP, pepTIRAP^{ALA}, and pepTAT

As mentioned before, the internalization mechanisms used by pepTAT and pepTIRAP seem to be dependent on their cationic clusters [29]. The effect of these clusters on the electrostatic surface potential of pepTAT and pepTIRAP is shown in Figs. 1A and 1B, where a predominantly positive EPF is found on the surface of both peptides. It has been reported that the replacement of cationic clusters with alanine decreases the internalization of pepTAT and pepTIRAP [29]. The lack of these cationic clusters in pepTIRAP^{ALA} produces a more balanced distribution of its EPF (Fig. 1C) when compared to pepTAT and pepTIRAP. The effect of these replacements in the EPF isosurfaces of magnitude -1 *kT*/*e* and +1 *kT*/*e* for the models is shown in Fig. 2. For pepTIRAP and pepTAT, these positive electrostatic isosurfaces extend further than the negative ones. Replacement of cationic amino acids with alanine, causes a reduction on the size of the positive electrostatic isosurface for pepTIRAP^{ALA}, making it comparable to the negative one.

Peptides rich in arginine, such as pepTAT and R9 are effectively internalized by cells [9,19]. It has been hypothesized that the internalization of arginine rich peptides is due to the guanidine head group present in arginine. This group would form bidentate hydrogen bonds with the anionic groups on the surface of the cell [48,49]. Therefore, replacement of these residues would cause diminished peptide internalization, as observed for pepTAT, where 5 out of 6 arginines were replaced with alanine [29]. For the case of pepTIRAP, 4 out of 5 lysines and only one out of two arginines were replaced with alanine. Lysine is a positively charged residue, but does not have a guanidine group. Replacement of arginine and lysine residues by alanine should not drastically change the peptides hydrophobicity, since alanine is a small, neutral amino acid. Even though it has been reported that lysine homopolymers are not efficiently internalized [50], replacement of the majority of the lysine residues and only one arginine

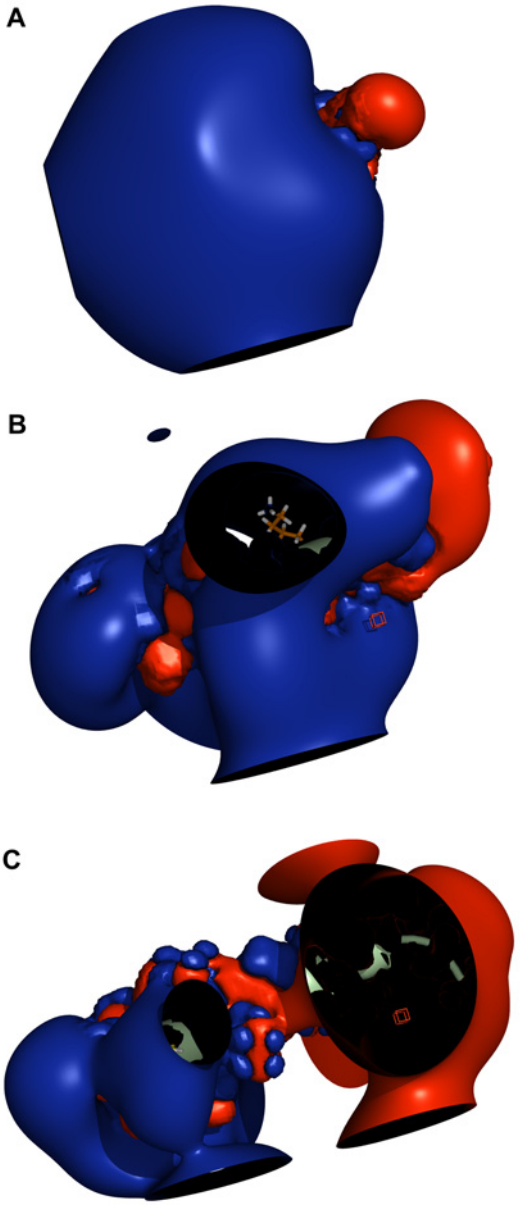

Fig. 2. Electrostatic potential isosurfaces with a magnitude of +1 and -1 *kT*/*e* for (A) pepTAT, (B) pepTIRAP, and (C) pepTIRAP^{ALA}. Electrostatic potential isosurfaces with a magnitude of +1 and -1 *kT*/*e* for (A) pepTAT, (B) pepTIRAP, and (C) pepTIRAP^{ALA}. Positive electrostatic potential with a magnitude +1 *kT*/*e* is colored blue, and potential with a magnitude of -1 *kT*/*e* is colored red. The figure shows that the positive electrostatic isosurfaces for pepTAT (A) and pepTIRAP (B) dominate the isosurface projection, with an extension far beyond than the negative isosurface. The mutation of cationic amino acids by alanines, in the case of pepTIRAP^{ALA} (C), reduced the size of its positive electrostatic isosurface, in this way, balancing the electrostatic potential distribution on the surface. Images were prepared using PyMol [41].

residue with alanines in pepTIRAP, has a significantly negative effect on its internalization [29]. As shown in the previous results, these mutations also causes a reduction in the positive electrostatic isosurfaces.

Based on these results, the main effect of the replacement of cationic clusters is the alteration on the characteristics of the peptides electrostatic potential. We postulate that due to its predominantly positive EPF, pepTIRAP interacts with molecules on the cell membrane, facilitating its internalization. The characteristics of the EPF in pepTIRAP^{ALA} result in weaker interactions with the cell membrane that decrease its internalization.

3.3. Docking experiments for pepTIRAP, pepTIRAP^{ALA}, and heparan sulfate

Blind docking experiments were performed using a grid box centered in the peptide, made large enough to accommodate the free movement of the ligand around all the peptides surface. Once the preferred binding area was located, specific docking experiments were carried out using a grid box centered in these interactions zones. Figs. 3A and 3B shows the final dockings of HS-dp4 to pepTIRAP and pepTIRAP^{ALA}, respectively. The best docking conformations of the HS-dp4 molecules are located over the surface of peptides where the electrostatic potential is positive. This fact points out the relevance of electrostatic interactions between the peptides and HS-dp4. Fig. 3C shows the detailed interactions on the docked conformation of HS-dp4 to pepTIRAP. Several hydrogen bond interactions between the peptide and HS-dp4 can be observed. The carboxylate moiety of the S1 ring interacts with the NH of Trp6 and with an hydrogen of the amide moiety of Gln9. Another hydrogen bond acceptor between the $-NH_3^+$ moiety of Lys13 and the hydroxyl group of S2 ring can be observed. Another hydrogen bond is shared between the side chain of Asn20 and the hydroxyl substituent of S3. Notice that the oxygen atoms of HS-dp4 act as acceptors of these hydrogen interactions. It is worth to mention that the hydrogen bond interaction between the NH_3^+ moiety of Lys17 and the carboxylate of S3 is reinforced by an electrostatic interaction between the positively charged amine group and the carboxylate. Also, the protonated amine of Lys17 interacts with the anomeric oxygen between sugar rings S3 and S4. In addition, two additional interactions are possible between Lys16 and the amide oxygen of S2 and the hydroxyl sugar of S3, due to the inherent movement associated with the side chain, which could shorten the average distance observed of 4.3 Å. The same argument is valid for the hydroxyl group of Thr25 and the closest hydroxyl group of S4.

Fig. 3D shows the detailed interactions on the docked conformation of HS-dp4 to pepTIRAP^{ALA}. Unlike

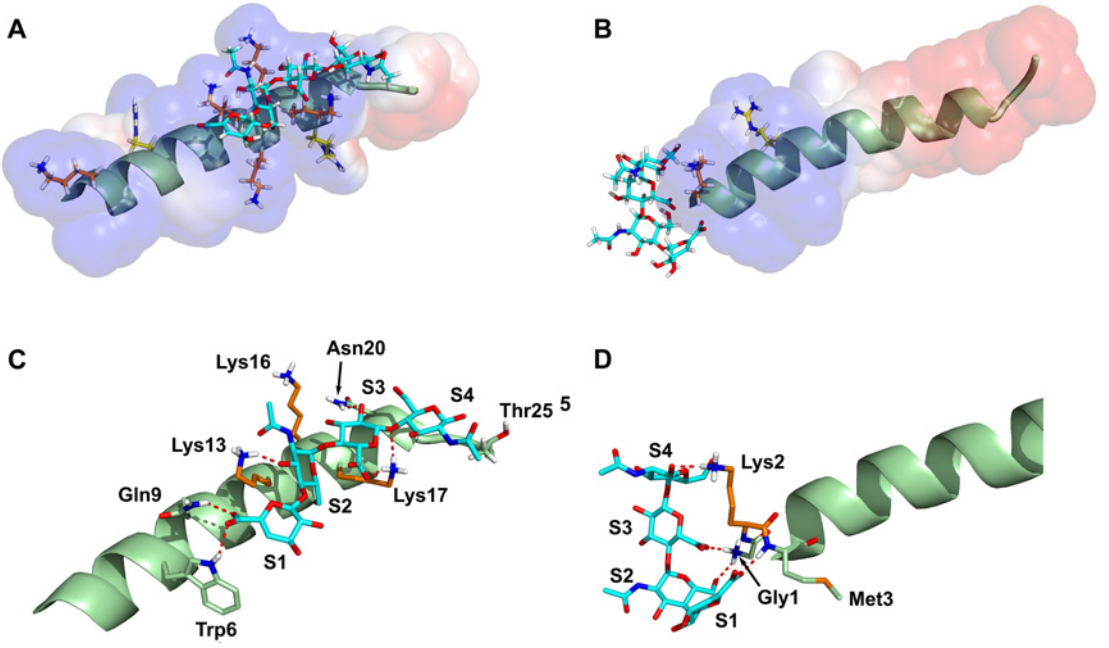

Fig. 3. Docking results. Final docked complexes for HS-dp4 with pepTIRAP (A) and pepTIRAP^{ALA} (B) are shown. The positive electrostatic potential on the surface of the peptides is colored blue, while the negative potential is colored in red. Cationic amino acids of the peptides are displayed using stick representation. The HS-dp4 molecule is shown with stick representation where carbons are colored cyan. Detailed interactions on the docked conformation of HS-dp4 to pepTIRAP and pepTIRAP^{ALA} are shown in (C) and (D) respectively. HS-dp4 rings are labeled as S1, S2, S3 and S4 respectively. For the sake of simplicity only residues and hydrogens relevant for the interaction in the complexes are depicted. Also, hydrogens belonging to HS-dp4 are omitted for simplicity. Dotted red lines indicate hydrogen bonds and electrostatic interactions. Images were prepared using PyMol [41].

pepTIRAP, only four hydrogen bond interactions are observed in this complex. The carboxylate group of S1 now interacts with the amide peptide hydrogen of Met3. Two additional interactions occur between a hydroxyl group of S2 and the carboxylate of S3 with the N-terminal moiety of the peptide corresponding to Gly1. As before, this hydrogen bond interaction is reinforced by electrostatic interations. The last interaction corresponds to the hydrogen bond between the hydroxyl group of S4 and the protonated amine group of Lys2. A distinct feature of this docking pose is the folded conformation adopted by HS-dp4 with pepTIRAP^{ALA} compared to the one obtained for pepTIRAP, and its preferred location at the beginning of the peptide. This docking pose might be due to the lack of lysine residues belonging to pepTIRAP which were replaced by alanines in pepTIRAP^{ALA}. These positively charged lysines create a favorable interaction surface for the negatively charged HS-dp4. Mutations on pepTIRAP^{ALA} decrease the available surface for favorable interactions.

Therefore, stabilization interactions estimated from pepTIRAP and pepTIRAP^{ALA} dockings indicate that the interactions between HS-dp4 and pepTIRAP is far more favorable than those observed between HS-dp4 and pepTIRAP^{ALA} due to the larger number of hydrogen bond and electrostatic interactions observed in the former case. These results support the hypothesis that interactions between pepTIRAP and negatively charged molecules on the cellular surface such as heparan sulfate are stronger than the ones exhibited by pepTIRAP^{ALA}.

3.4. Cellular viability and peptide concentration threshold

Experimental fluorescence measurements for HeLa cells after incubation with pepTIRAP and pepTIRAP^{ALA} 10, 40, and 100 μM are shown in Fig. 4. An increase in propidium iodide (PI) fluorescence is observed as pepTIRAP concentration is increased. This is not the case for pepTIRAP^{ALA} where an increase in peptide concentration does not cause noticeable changes in fluorescence. In these experiments fluorescence intensity correlates with cell death, therefore an increment on the peptide concentration during incubation leads to higher levels of cell death. There is a marked increase in fluorescence when cells are incubated with pepTIRAP at concentrations above 40 μM. The fraction of dead cells (PI^+), *i.e.* with fluorescence higher than the autofluorescence, increases from 14.5 to 31.5%.

Fig. 4 shows cell viability for incubation with pepTIRAP and pepTIRAP^{ALA} at concentrations ranging from 0 to 100 μM. The average viability of live control cultures (LC) was 87.9%. Cell viability decreases with increasing concentrations of pepTIRAP. No such changes are observed in the case of pepTIRAP^{ALA}. There is a significant decrease in cell viability for pepTIRAP concentrations above 40 μM ($p < 0.05$, no parametric t-Student 1 and 2 tails). For concentrations above 40 μM of pepTIRAP there is an average decrease in cell viability of 23.5% compared to LC cultures. In the case of staurosporine treated apoptotic controls (AC) the average decrease in cell viability was 12.7% (data not shown). Incubation with pepTIRAP^{ALA} did

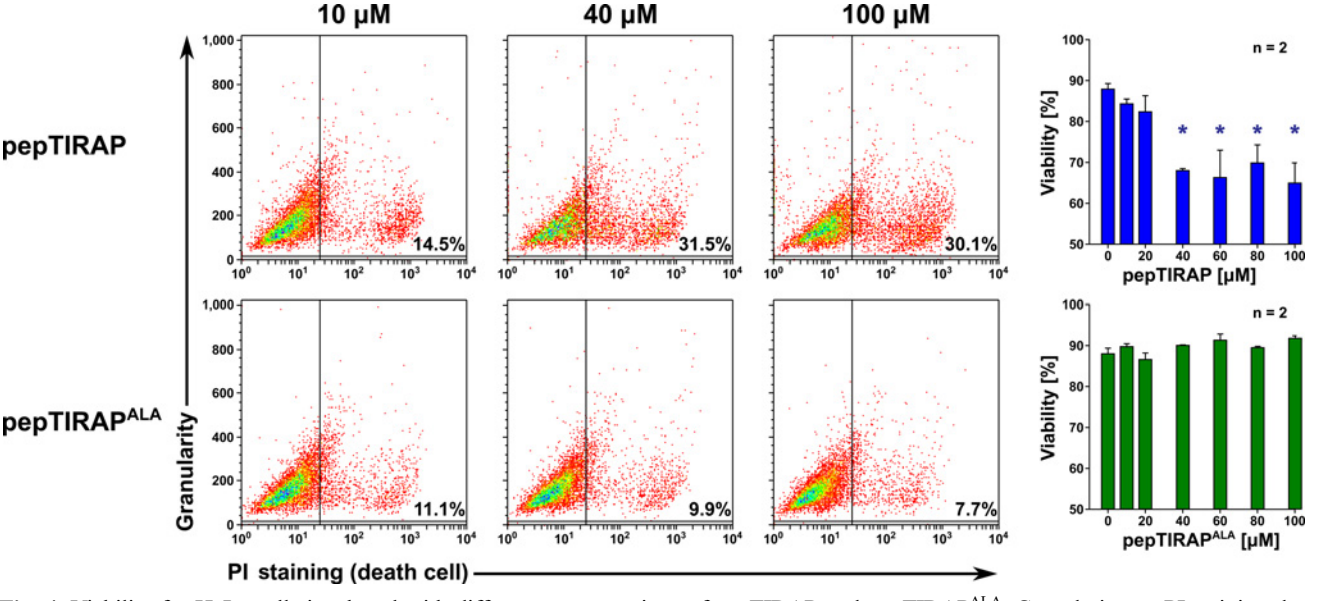

Fig. 4. Viability for HeLa cells incubated with different concentrations of pepTIRAP and pepTIRAP^{ALA}. Granularity *vs*. PI staining dot plots, and viability for HeLa cells incubated for 16 h with pepTIRAP or pepTIRAP^{ALA} at 10, 40, and 100 μM. Bar plots show the average viability for 2 independent experiments and their respective standard errors. Asterisks indicate significant differences compared to live control cultures (LC) (no parametric t-Student 1 and 2 tails). The vertical line marks the autofluorescence threshold for viable cells. The average viability of live control cultures (LC) was 87.9%. For concentrations above 40 μM pepTIRAP viability decreases below 80%.

not affect cell viability, since there is no significant difference ($p > 0.05$, no parametric t-Student 1 and 2 tails) when compared to LC cultures. A concentration of 40 μM of peptide was identified as the threshold for viability, and selected for the following internalization experiments.

It has been previously reported that the internalization mechanism of pepTAT in HeLa cells changes from endocytosis to transduction at peptide concentrations above 10 μM, producing a strong enhancement of the cytoplasmatic delivery of peptides [19]. Based on this evidence, we propose that the increment of cell death observed at 40 μM of pepTIRAP, is related to a change in the internalization mechanism used by pepTIRAP, which produces an increment in the cytoplasmatic delivering of the peptide, triggering cell death. The EPF isosurface for the pepTAT model is larger than the one for pepTIRAP. In fact, the cationic clusters in pepTAT represent 61.5% of the amino acids on the sequence compared to 28.0% for pepTIRAP. This fact may explain the differences in the threshold concentration required for transduction for each peptide.

3.5. Peptide internalization

The previous section shows that pepTIRAP has a negative effect on cellular viability. In this section we explore the internalization of this peptide. To determine and quantify peptide internalization, pepTIRAP and pepTIRAP^{ALA} were labeled with biotin, which specifically binds to streptavidin-R-PE (STR-R-PE). The degree of internalization is determined by flow cytometry.

It has been reported that STR-R-PE can associate non-specifically to non-biotinylated compounds on the cell membrane as illustrated in Fig. 5A. STR-R-PE contains the triplet Arg-Tyr-Asp (RYD) that mimics the triplet Arg-Gly-Asp (RGD), known as fibronectin-binding sequence [51]. This sequence binds to integrins and other molecules related to the cell surface [52,53]. In addition, STR-R-PE can specifically bind to biotinylated peptides located outside the cell (see Fig. 5B), to internalized biotinylated peptides (see Fig. 5C), and other endogenously biotinylated proteins in the intracellular space and mitochondria as depicted in Fig. 5D [54]. Biotin's presence inside the cell is due to its involvement in important metabolic pathways, such as gluconeogenesis, fatty acid synthesis and amino acids catabolism [55]. Therefore, total measured fluorescence corresponds to the sum of all these interactions, specific and non-specific.

In order to determine the fluorescence associated to specific interactions of STR-R-PE to biotinylated peptides it is necessary to quantify the other specific and non-specific interactions. To quantify non-specific associations of STR-R-PE to membrane bound compounds, cells were directly exposed to STR-R-PE (NFP control) and fluorescence was measured. For determining the specific association of STR-R-PE to endogenously biotinylated compounds, cells

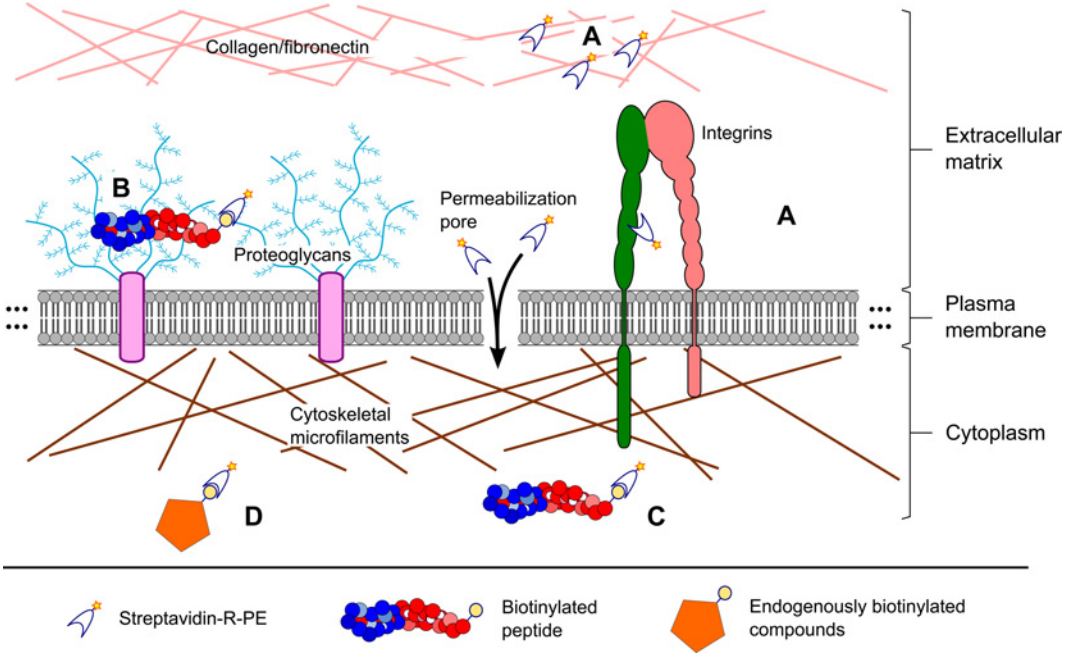

Fig. 5. Specific and non-specific interactions of Streptavidin-R-PE. Figure shows all the specific and non-specific interactions of Streptavidin-R-PE considered. (A) Non-specific binding to extracellular matrix components, (B) specific binding to membrane bound biotinylated peptides, (C) specific binding to internalized biotinylated peptides, (D) specific binding to endogenously biotinylated compounds.

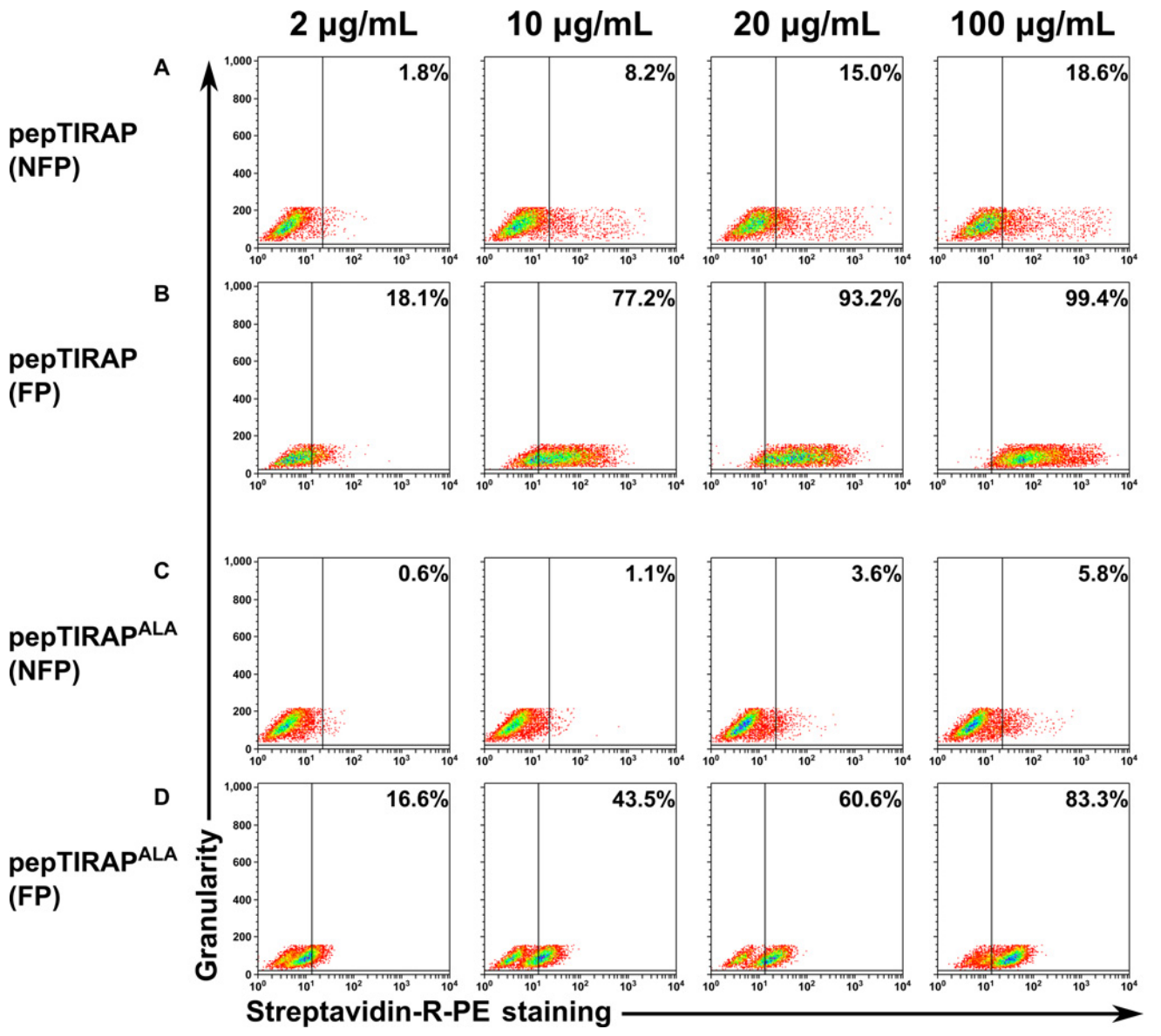

Fig. 6. Peptide detection, after incubation with pepTIRAP and pepTIRAP^{ALA} for 2 h in HeLa cells. Granularity *vs*. Streptavidin-R-PE staining dot plots for HeLa cells incubated for 2 h with 40 µM pepTIRAP or pepTIRAP^{ALA}, with Streptavidin-R-PE concentrations of 2, 10, 20, and 100 µg/mL. (A) Incubation of non-permeabilized cells with pepTIRAP, (B) incubation of permeabilized cells with pepTIRAP, (C) incubation of non-permeabilized cells with pepTIRAP^{ALA}, (D) incubation of permeabilized cells with pepTIRAP^{ALA}. The vertical line marks the autofluorescence threshold for viable cells.

were permeabilized and fixed, exposed to STR-R-PE (FP control) and fluorescence was measured.

Experimental fluorescence measurements after incubation with pepTIRAP 40 µM are shown in Figs. 6A and 6B for STR-R-PE concentrations 2, 10, 20, and 100 µg/mL. Increasing concentrations of STR-R-PE are used to build a saturation curve for biotinylated peptides detection. Fig. 6A shows results for cells without fixation-permeabilization treatment (NFP). Without permeabilization, STR-R-PE is unable to enter the cells, and only binds specifically to peptides associated to the extracellular membrane, and non-specifically to the extracellular matrix. Therefore, measured fluorescence corresponds to the sum of specific and non-specific interactions illustrated in Figs. 5B and 5A, respectively. 18.6% of the non-permeabilized cells are above the fluorescence threshold for 100 µM STR-R-PE. Experimental results for cell with fixation-permeabilization treatment (FP) are shown in Fig. 6B. Since the membrane is permeabilized, STR-R-PE can enter the cells and additionally bind specifically to biotinylated peptides and endogenously biotinylated compounds. In this case measured fluorescence corresponds to the sum of specific and non-

specific interactions, both extracellular and intracellular, as depicted in Fig. 5. 99.4% of the permeabilized cells are above the fluorescence threshold for 100 μM STR-R-PE. An increase in fluorescence is observed in Fig. 6A with increasing concentrations of STR-R-PE as it binds to pepTIRAP and other extracellular compounds. There is an heterogeneous fluorescence distribution for events above the autofluorescence threshold, with fluorescence intensity ranging from 10^0 to 10^4 a.u.. This suggests a diverse amount of peptide located on the cell membrane among the population. The increase in fluorescence with increasing concentrations of STR-R-PE shown in Fig. 6B is higher than the one in Fig. 6A, since STR-R-PE is detecting in addition to extracellular interactions, intracellular biotinylated compounds. Heterogeneity in fluorescence distribution for events above the autofluorescence threshold is similar to the case of non-permeabilized cells, with fluorescence intensity ranging from 10^1 to 10^4 a.u.. Considering that endogenously biotinylated compounds are distributed homogeneously in the cell population, fluorescence distribution heterogeneity can be attributed to differences in the degree of pepTIRAP internalization. This phenomenon has also been observed in cultures with the cationic peptides pepTAT and R9 [19].

Figures. 6C and 6D show experimental fluorescence measurements after incubation with pepTIRAP^{ALA} 40 μM for STR-R-PE concentrations 2, 10, 20, and 100 μg/mL. The increase in fluorescence with increasing concentrations of STR-R-PE for non-permeabilized cells, is also observed as for the case of pepTIRAP (Fig. 6C). However, the lower percentage (5.8%) of the population above the autofluorescence threshold and the narrower distribution range (10^0 ~ 10^2 a.u.) indicates a weaker interaction of pepTIRAP^{ALA} with the cellular membrane compared to pepTIRAP, since non-specific interactions are comparable in both cases. Experimental results for permeabilized cells incubated with pepTIRAP^{ALA} in Fig. 6D show lower increase in the percentage of events above the autofluorescence threshold compared to pepTIRAP. In fact, the distribution range (10^0 ~ 10^2 a.u.) is similar to the one obtained for FP controls (data not shown). This indicates a lower internalization of pepTIRAP^{ALA} compared to pepTIRAP, as expected.

Mean fluorescence intensity model. In order to analyze the mean fluorescence intensity (*MFI*) and the contribution of each of its components to the total measured fluorescence, a mathematical model is proposed. The model considers both specific and non-specific interactions for STR-R-PE illustrated in Fig. 5, and allows the quantification of biotinylated peptides located inside and outside the cell. The total fluorescence measured is the result of specific (MFI_S) and non-specific (MFI_{NS}) interactions. To build the model we consider non-specific associations to be directly proportional to STR-R-PE concentration, and that specific associations follow a saturation curve.

The fluorescence due to specific binding of STR-R-PE to a biotinylated compound j, $MFI_S(j)$, is described by the following saturation expression, similar to a Michaelis-Menten equation [56]:

$$MFI_S(j) = \frac{MFI_{max}(j) \cdot S}{K_d + S} \quad (1)$$

where S is the STR-R-PE incubation concentration, MFI_{max} is the maximum fluorescence associated to compound j, and K_d is the STR-R-PE concentration where half of the maximum fluorescence is achieved, and represents its affinity for biotin. For high STR-R-PE concentrations ($S \rightarrow \infty$), the maximum fluorescence MFI_{max} is achieved.

The non-specific association also follows a saturation curve, but it saturates at significantly higher concentrations of STR-R-PE. Therefore, fluorescence associated to the non-specific binding of streptavidin to extracellular matrix components, MFI_{NS}, can be approximated by the following linear equation:

$$MFI_{NS} = AF + NS \cdot S \quad (2)$$

where AF and NS correspond to the autofluorescence and non-specific binding affinity, respectively.

This way, the mean fluorescence intensity (*MFI*) is given by the sum of Equations 1 and 2:

$$MFI = AF + NS \cdot S + \frac{MFI_{max} \cdot S}{K_d + S} \quad (3)$$

In order to estimate the model parameters: AF, NS, K_d and MFI_{max}, Equation 3 was fitted to the experimental *MFI* (Fig. 7) using a nonlinear regression method available in a commercial package. Results are shown in Table 2. The binding constant (K_d) is specific to the STR-R-PE and biotin interaction, the non-specific affinity (NS) and autofluorescence (AF) are a characteristic of the cellular system used. The values estimated using the fitting process are similar for all experiments, showing coherence in all parameters which are independent of the peptide used.

Figure 7 show experimental and simulated values of *MFI* for pepTIRAP, pepTIRAP^{ALA} and controls, in the case of permeabilized (FP) and non-permeabilized cell (NFP). There is a very good agreement between the model and experimental data in all cases. For pepTIRAP in Fig. 7A, the difference between pepTIRAP FP and control FP curves show that a large amount of pepTIRAP is entering the cell. The difference between pepTIRAP NFP and control NFP curves show the fluorescence attributable to membrane bound pepTIRAP. In the case of pepTIRAP NFP experiments most of the fluorescence detected is due to peptide bound to the membrane. MFI values for

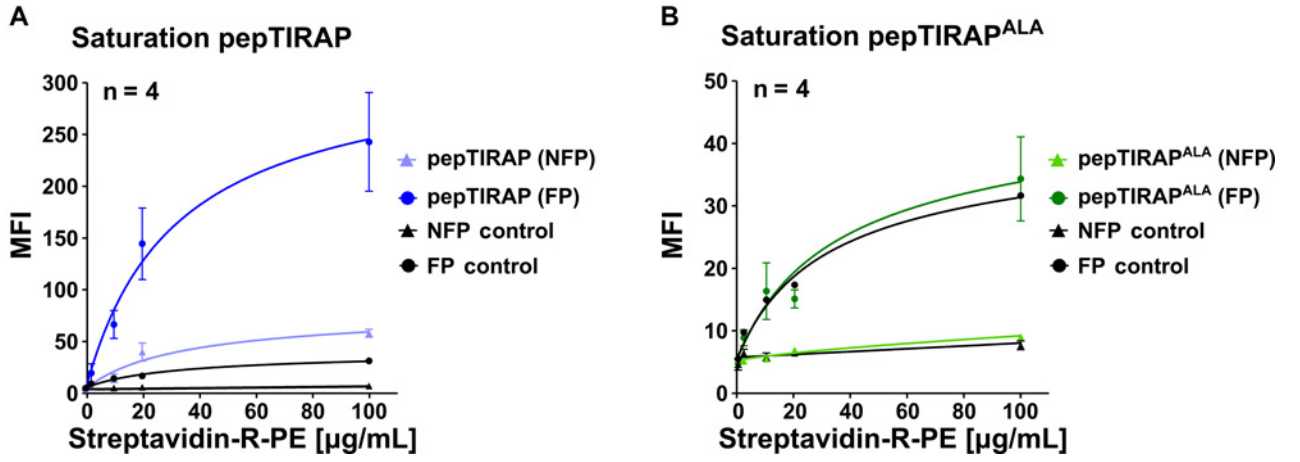

Fig. 7. MFI model *vs*. experimental data. MFI model simulation and mean fluorescence intensity calculated for all experimental conditions. (A) Incubation with 40 µM pepTIRAP, (B) incubation with 40 µM pepTIRAP^{ALA}. Symbols indicate average experimental MFI and their corresponding standard error. Lines correspond to the simulation of the MFI model.

Table 2. Best-fit parameters and standard error for the *MFI* model for all experimental conditions

		Total binding[a]				Non-specific binding	
Parameter	Control (FP)	pepTIRAP (FP)	pepTIRAP^{ALA} (FP)	pepTIRAP (NFP)	pepTIRAP^{ALA} (NFP)	Average[c]	Control (NFP)
MFI_{max}	30.3[b] ± 3.50	311.0 ± 53.8	33.97 ± 8.80	68.36 ± 11.7	1.78 ± 2.5	NA	NA
K_d	28.6 ± 7.26	30.9 ± 11.3	31.3 ± 17.7	31.3 ± 11.3	34.7 ± 98.9	31.35 ± 0.63	NA
NS	0.019 ± 0.01	0.028 ± 0.22	0.023 ± 0.035	0.028 ± 0.047	0.026 ± 0.007	0.025 ± 0.023	0.02 ± 0.03
AF	5.77 ± 0.47	4.01 ± 6.74	5.59 ± 1.09	4.55 ± 1.46	5.10 ± 0.25	5.04 ± 0.32	5.23 ± 0.90

[a]Single site binding was considered for Streptavidin-R-PE.
[b]MFI_{max} for FP control represents the maximum amount of Streptavidin-R-PE bound to endogenously biotinylated compounds.
[c]Average values of *MFI* model parameters for all experimental conditions.

pepTIRAP^{ALA} in Fig. 7B are considerably lower than the ones for pepTIRAP (notice the difference in scale). The insignificant difference between pepTIRAP^{ALA} FP and control FP curves indicate that the peptide barely enters the cell. Moreover, in the case of NFP experiments results show that pepTIRAP^{ALA} has a weak interaction with the cell membrane.

In order to isolate the fluorescence due to biotinylated peptide outside and inside the cell, from the total fluorescence measured, detailed equations for all the components involved in FP and NFP experiments are presented.

The non-specific binding of STR-R-PE to extracellular matrix components in the NFP control, $MFI_{NS}^{NFP}(control)$, is given by the following equation:

$$MFI_{NS}^{NFP}(control) = AF + NS \cdot S \tag{4}$$

where *AF* and *NS* correspond to the parameter values found in Table 2.

In the case of FP controls, fluorescence detected is due to specific binding of STR-R-PE to endogenously biotinylated compounds inside the cell (MFI_S^{EB}) and non-specific binding to extracellular matrix components. Therefore,

$$MFI^{FP}(control) = MFI_S^{EB} + MFI_{NS}^{NFP}(control) \tag{5}$$

where the specific association represented by MFI_S^{EB} follows Equation 1.

The *MFI* for FP cultures with peptide ($MFI^{FP}(peptide)$) is the result of the contributions of internalized $MFI_S^{int}(peptide)$ and membrane bound peptide $MFI_S^{ext}(peptide)$, endogenously biotinylated compounds and non-specific binding to extracellular matrix components.

$$MFI^{FP}(peptide) = MFI_S^{int}(peptide) + MFI_S^{ext}(peptide) + MFI_S^{EB} + MFI_{NS}^{NFP}(control) \tag{6}$$

For NFP cultures incubated with peptide $MFI^{NFP}(peptide)$, *MFI* is the result of contributions of membrane bound peptide $MFI_S^{ext}(peptide)$ and non-specific binding to extracellular matrix components, as given by

$$MFI^{NFP}(peptide) = MFI_S^{ext}(peptide) + MFI_{NS}^{NFP}(control) \quad (7)$$

Notice that $MFI_S^{int}(peptide)$ and $MFI_S^{ext}(peptide)$ also follow the expression in Equation 1.

Given that non-specific contributions are independent of the peptide and permeabilization treatment, it is possible to remove these terms from Equations 5, 6 and 7, and establish a balance considering only specific interactions:

$$MFI_S^{FP}(control) = MFI_S^{EB} \quad (8)$$

$$MFI_S^{FP}(peptide) = MFI_S^{int}(peptide) + MFI_S^{ext}(peptide) + MFI_S^{EB} \quad (9)$$

$$MFI_S^{NFP}(peptide) = MFI_S^{ext}(peptide) \quad (10)$$

Moreover, the case of high concentrations of STR-R-PE, where all biotinylated compounds are bound, can be represented by S concentration growing to infinity. Replacing the expression in Equation 1 and taking the limit as $S \rightarrow \infty$, the previous system of equations is simplified to:

$$MFI_{max}^{FP}(control) = MFI_{max}^{EB} \quad (11)$$

$$MFI_{max}^{FP}(peptide) = MFI_{max}^{EB} + MFI_{max}^{int}(peptide) + MFI_{max}^{ext}(peptide) \quad (12)$$

$$MFI_{max}^{NFP}(peptide) = MFI_{max}^{ext}(peptide) \quad (13)$$

Therefore, the maximum fluorescence that can be associated to endogenously biotinylated compounds in HeLa cells MFI_{max}^{EB} is determined from MFI_{max} for FP control experiments in Table 2, and it is equal to $MFI_{max}^{FP}(control)$. The maximum fluorescence associated to membrane bound biotinylated peptide $MFI_{max}^{ext}(peptide)$ is determined from MFI_{max} for NFP experiments in the presence of peptide in Table 2, and it is equal to $MFI_{max}^{NFP}(peptide)$. The only remaining unknown term is the maximum fluorescence of internalized biotinylated peptide $MFI_{max}^{int}(peptide)$ and it can be calculated from Equation 12.

The maximum fluorescence of the internalized and membrane bound peptide determined as described above, is shown in Fig. 8. The maximum fluorescence associated to pepTIRAP located outside the plasma membrane is almost 40-fold higher than that for pepTIRAP^{ALA}. In the case of internalized peptide, this difference is even higher. Internalized pepTIRAP is more than a hundred times higher than internalized pepTIRAP^{ALA}. According to these results, pepTIRAP is highly internalized in HeLa cells after 2 h of incubation. In contrast pepTIRAP^{ALA} binds poorly

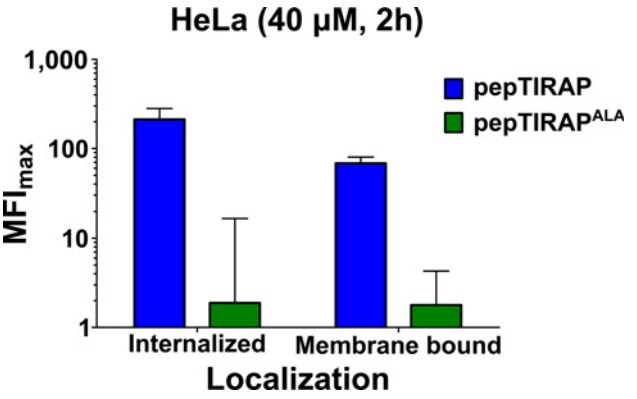

Fig. 8. Quantification of internalized and membrane bound peptide. Amount of internalized and membrane bound peptide estimated by the *MFI* model for cultures incubated with 40 μM pepTIRAP or pepTIRAP^{ALA}. Bars show the maximum mean fluorescence intensity (MFI_{max}) in logarithmic scale. Standard errors are obtained from Table 2. In the case of internalized peptides, they are calculated as the sum of the appropriate standard errors.

and scarcely crosses the plasma membrane. The maximum fluorescence associated to internalized pepTIRAP is 3-fold the fluorescence associated to pepTIRAP located on the membrane. In spite the fact that pepTIRAP is highly internalized, the amount of peptide bound to the membrane is considerable, suggesting that pepTIRAP can establish strong interactions with the cell membrane. To our knowledge, this is the first experimental evidence that quantifies the strong association of pepTIRAP to the plasma membrane.

These results relate to the first stage of the transduction internalization mechanism: binding of the peptide to the membrane and formation of nucleation zones. PepTIRAP displays a predominantly positive potential on its surface when compared to pepTIRAP^{ALA}, which has a more balanced distribution of EPF. We propose that due to its positive potential pepTIRAP interacts with molecules on the cell membrane, such as proteoglycans and phospholipid heads [49,57], facilitating the formation of nucleation zones that are key in the transduction internalization mechanism. Since pepTIRAP^{ALA} does not display such a high positive potential, its interactions with the membrane are weaker, and may not allow the formation of nucleation zones. This hypothesis is also supported by the results given by the docking experiments between peptides and Heparan Sulfate, where stabilization interactions estimated from pepTIRAP dockings are more favorable that those from pepTIRAP^{ALA}. Fig. 9 shows a diagram of the proposed internalization mechanism. At high peptide concentration, the strong interactions between pepTIRAP and molecules on the surface of the plasma membrane produce local accumulation of the peptide, forming nucleation zones. This promotes the reorganization of the

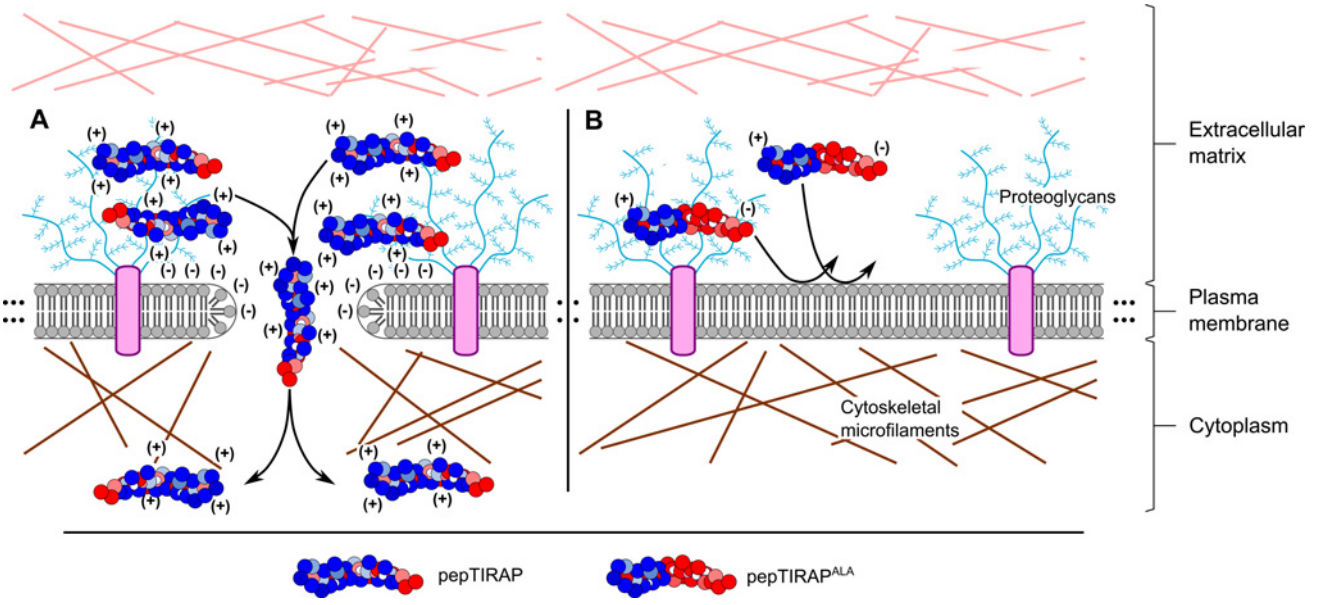

Fig. 9. Internalization mechanism proposed for pepTIRAP and pepTIRAP^{ALA}. (A) Interaction of the electrostatic potential of pepTIRAP with molecules on the plasma membrane at high peptide concentrations, produces local accumulation of peptide on the membrane surface. This generates nucleation zones followed by the reorganization of the actin cytoskeleton, leading to a change in membrane fluidity and the subsequent internalization of pepTIRAP. (B) PepTIRAP^{ALA} establishes weak interactions with the plasma membrane due to the characteristics of its electrostatic potential, hence the peptide is not internalized.

actin cytoskeleton leading to a change in membrane fluidity, which results on the internalization of the peptide. Therefore, the transduction mechanism does not depend only on peptide concentration [19,29], but also on the electrostatic potential on the surface of the peptide.

4. Conclusion

In this work, we studied the internalization mechanism of a peptide derived from the TIRAP protein (pepTIRAP), and pepTIRAP^{ALA}, where some of its cationic amino acids were changed to alanine, in order to identify the effect of changes in electrostatic potential on peptide internalization. Molecular modeling studies showed that the replacement of cationic amino acids with alanine, resulted in a decrease in the positive electrostatic potential in the peptide, even when its three dimensional structure remains mostly unaltered. Also, docking experiments show that interactions between pepTIRAP and negatively charged molecules on the cellular surface, such as heparan sulfate, are stronger than the ones exhibited by pepTIRAP^{ALA}.

Experimental results indicate that pepTIRAP concentration has an effect on cell viability, which is reduced as concentration increases. This is not observed for pepTIRAP^{ALA}. Flow cytometry results show that pepTIRAP enters the cell, while pepTIRAP^{ALA} is not considerably internalized. In addition, at the same concentration pepTIRAP binds to the membrane to a greater extent than pepTIRAP^{ALA}.

A mathematical model was developed which allows the quantification of the amount of peptide that is internalized and the amount bound to the membrane, based on flow cytometry measurements. Using this model we determined that the amount of pepTIRAP internalized is in the same order of magnitude than the amount found bound to the membrane, and that this is over a hundred times higher than the amount of pepTIRAP^{ALA} that enters the cell.

Based on this evidence, we propose that the difference in internalization between pepTIRAP and pepTIRAP^{ALA} is due mainly to differences in their electrostatic potential, suggesting that a mechanism dependent on the electrostatic interactions between the peptide and molecules on the membrane, is triggering peptide internalization. Moreover, the high amount of pepTIRAP found associated to the membrane is consistent with peptides entering the cell *via* a transduction mechanism.

Acknowledgements

This work was partially supported by FONDECYT Research Initiation Grants 11080016 and 11090268, the Millennium Scientific Initiative ICM project P05-001-F, and FONDECYT Grants 1080006 and 1080290.

Nomenclature

AF	:Autofluorescence
j	:Biotinylated compound *j*
K_d	:STR-R-PE concentration where half of the maximum fluorescence is achieved
MFI	:Mean fluorescence intensity
MFI_{max}	:Maximum fluorescence
NS	:Non-specific binding affinity
S	:STR-R-PE incubation concentration
EB	:Endogenously biotinylated compounds
int	:Internalized
ext	:No internalized
FP	:With fixation-permeabilization treatment
NFP	:Without fixation-permeabilization treatment
NS	:Non-specific interactions
S	:Specific interactions

References

1. Nori, A., K. D. Jensen, M. Tijerina, P. Kopeckova, and J. Kopecek (2003) Tat-conjugated synthetic macromolecules facilitate cytoplasmic drug delivery to human ovarian carcinoma cells. *Bioconjug. Chem*. 14: 44-50.
2. Choi, M., S. Rolle, M. Wellner, M. C. Cardoso, C. Scheidereit, F. C. Luft, and R. Kettritz (2003) Inhibition of NF-κB by a TAT-NEMO-binding domain peptide accelerates constitutive apoptosis and abrogates LPS-delayed neutrophil apoptosis. *Blood* 102: 2259-2267.
3. Fawell, S., J. Seery, Y. Daikh, C. Moore, L. L. Chen, B. Pepinsky, and J. Barsoum (1994) Tat-mediated delivery of heterologous proteins into cells. *Proc. Natl. Acad. Sci. U. S. A*. 91: 664-668.
4. Turner, J. J., G. D. Ivanova, B. Verbeure, D. Williams, A. A. Arzumanov, S. Abes, B. Lebleu, and M. J. Gait (2005) Cell-penetrating peptide conjugates of peptide nucleic acids (PNA) as inhibitors of HIV-1 Tat-dependent trans-activation in cells. *Nucleic Acids Res*. 33: 6837-6849.
5. Lewin, M., N. Carlesso, C. H. Tung, X. W. Tang, D. Cory, D. T. Scadden, and R. Weissleder (2000) Tat peptide-derivatized magnetic nanoparticles allow in vivo tracking and recovery of progenitor cells. *Nat. Biotechnol*. 18: 410-414.
6. Joliot, A., C. Pernelle, H. Deagostini-Bazin, and A. Prochiantz (1991) Antennapedia homeobox peptide regulates neural morphogenesis. *Proc. Natl. Acad. Sci. U. S. A*. 88: 1864-1868.
7. Frankel, A. D. and C. O. Pabo (1988) Cellular uptake of the tat protein from human immunodeficiency virus. *Cell* 55: 1189-1193.
8. Malecki, J., J. Wesche, C. S. Skjerpen, A. Wiedlocha, and S. Olsnes (2004) Translocation of FGF-1 and FGF-2 across vesicular membranes occurs during G1-phase by a common mechanism. *Mol. Biol. Cell* 15: 801-814.
9. Tunnemann, G., G. Ter-Avetisyan, R. M. Martin, M. Stockl, A. Herrmann, and M. C. Cardoso (2008) Live-cell analysis of cell penetration ability and toxicity of oligo-arginines. *J. Pept. Sci*. 14: 469-476.
10. Yoshikawa, T., T. Sugita, Y. Mukai, Y. Abe, S. Nakagawa, H. Kamada, S. Tsunoda, and Y. Tsutsumi (2009) The augmentation of intracellular delivery of peptide therapeutics by artificial protein transduction domains. *Biomaterials* 30: 3318-3323.
11. Deshayes, S., M. C. Morris, G. Divita, and F. Heitz (2005) Cell-penetrating peptides: tools for intracellular delivery of therapeutics. *Cell. Mol. Life Sci*. 62: 1839-1849.
12. Suzuki, T., S. Futaki, M. Niwa, S. Tanaka, K. Ueda, and Y. Sugiura (2002) Possible existence of common internalization mechanisms among arginine-rich peptides. *J. Biol. Chem*. 277: 2437-2443.
13. Vives, E., P. Brodin, and B. Lebleu (1997) A truncated HIV-1 Tat protein basic domain rapidly translocates through the plasma membrane and accumulates in the cell nucleus. *J. Biol. Chem*. 272: 16010-16017.
14. Derossi, D., S. Calvet, A. Trembleau, A. Brunissen, G. Chassaing, and A. Prochiantz (1996) Cell internalization of the third helix of the Antennapedia homeodomain is receptor-independent. *J. Biol. Chem*. 271: 18188-18193.
15. Richard, J. P., K. Melikov, H. Brooks, P. Prevot, B. Lebleu, and L. V. Chernomordik (2005) Cellular uptake of unconjugated TAT peptide involves clathrin-dependent endocytosis and heparan sulfate receptors. *J. Biol. Chem*. 280: 15300-15306.
16. Kaplan, I. M., J. S.Wadia, and S. F. Dowdy (2005) Cationic TAT peptide transduction domain enters cells by macropinocytosis. *J. Control. Release* 102: 247-253.
17. Console, S., C. Marty, C. Garcia-Echeverria, R. Schwendener, and K. Ballmer-Hofer (2003) Antennapedia and HIV transactivator of transcription (TAT) "protein transduction domains" promote endocytosis of high molecular weight cargo upon binding to cell surface glycosaminoglycans. *J. Biol. Chem*. 278: 35109-35114.
18. Fischer, R., K. Kohler, M. Fotin-Mleczek, and R. Brock (2004) A stepwise dissection of the intracellular fate of cationic cell-penetrating peptides. *J. Biol. Chem*. 279: 12625-12635.
19. Duchardt, F., M. Fotin-Mleczek, H. Schwarz, R. Fischer, and R. Brock (2007) A comprehensive model for the cellular uptake of cationic cell-penetrating peptides. *Traffic* 8: 848-866.
20. Tunnemann, G., R. M. Martin, S. Haupt, C. Patsch, F. Edenhofer, and M. C. Cardoso (2006) Cargo-dependent mode of uptake and bioavailability of TAT-containing proteins and peptides in living cells. *FASEB J*. 20: 1775-1784.
21. Wadia, J. S., R. V. Stan, and S. F. Dowdy (2004) Transducible TAT-HA fusogenic peptide enhances escape of TAT-fusion proteins after lipid raft macropinocytosis. *Nat. Med*. 10: 310-315.
22. Horng, T., G. M. Barton, R. A. Flavell, and R. Medzhitov (2002) The adaptor molecule TIRAP provides signalling specificity for Toll-like receptors. *Nature* 420: 329-333.
23. Toshchakov, V. U., S. Basu, M. J. Fenton, and S. N. Vogel (2005) Differential involvement of BB loops of toll-IL-1 resistance (TIR) domain-containing adapter proteins in TLR4- versus TLR2-mediated signal transduction. *J. Immunol*. 175: 494-500.
24. Takeda, K., T. Kaisho, and S. Akira (2003) Toll-like receptors. *Annu. Rev. Immunol*. 21: 335-376.
25. Schnare, M., G. M. Barton, A. C. Holt, K. Takeda, S. Akira, and R. Medzhitov (2001) Toll-like receptors control activation of adaptive immune responses. *Nat. Immunol*. 2: 947-950.
26. Medzhitov, R., P. Preston-Hurlburt, E. Kopp, A. Stadlen, C. Chen, S. Ghosh, and C. A. Janeway Jr. (1998) MyD88 is an adaptor protein in the hToll/IL-1 receptor family signaling pathways. *Mol. Cell* 2: 253-258.
27. Horng, T., G. M. Barton, and R. Medzhitov (2001) TIRAP: An adapter molecule in the Toll signaling pathway. *Nat. Immunol*. 2: 835-841.
28. Yamamoto, M., S. Sato, H. Hemmi, H. Sanjo, S. Uematsu, T. Kaisho, K. Hoshino, O. Takeuchi, M. Kobayashi, T. Fujita, K. Takeda, and S. Akira (2002) Essential role for TIRAP in activation of the signalling cascade shared by TLR2 and TLR4. *Nature* 420: 324-329.
29. Low, W., A. Mortlock, L. Petrovska, T. Dottorini, G. Dougan, and

A. Crisanti (2007) Functional cell permeable motifs within medically relevant proteins. *J. Biotechnol*. 129: 555-564.
30. Shi, J., T. L. Blundell, and K. Mizuguchi (2001) FUGUE: sequence-structure homology recognition using environment-specific substitution tables and structure-dependent gap penalties. *J. Mol. Biol*. 310: 243-257.
31. Mizuguchi, K., C. M. Deane, T. L. Blundell, M. S. Johnson, and J. P. Overington (1998) JOY: Protein sequence-structure representation and analysis. *Bioinformatics* 14: 617-623.
32. Bernstein, F. C., T. F. Koetzle, G. J. Williams, E. F. Meyer Jr., M. D. Brice, J. R. Rodgers, O. Kennard, T. Shimanouchi, and M. Tasumi (1977) The Protein Data Bank: A computer-based archival file for macromolecular structures. *J. Mol. Biol*. 112: 535-542.
33. Eswar, N., B. Webb, M. A. Marti-Renom, M. S. Madhusudhan, D. Eramian, M. Y. Shen, U. Pieper, and A. Sali (2006) Comparative protein structure modeling using Modeller. *Curr. Protoc. Bioinformatics* Chapter 5: Unit 5.6.
34. Marti-Renom, M. A., A. C. Stuart, A. Fiser, R. Sanchez, F. Melo, and A. Sali (2000) Comparative protein structure modeling of genes and genomes. *Annu. Rev. Biophys. Biomol. Struct*. 29: 291-325.
35. Fiser, A., R. K. Do, and A. Sali (2000) Modeling of loops in protein structures. *Protein Sci*. 9: 1753-1773.
36. Sali, A. and T. L. Blundell (1993) Comparative protein modelling by satisfaction of spatial restraints. *J. Mol. Biol*. 234: 779-815.
37. Willard, L., A. Ranjan, H. Zhang, H. Monzavi, R. F. Boyko, B. D. Sykes, and D. S. Wishart (2003) VADAR: A web server for quantitative evaluation of protein structure quality. *Nucleic Acids Res*. 31: 3316-3319.
38. Davis, I. W., A. Leaver-Fay, V. B. Chen, J. N. Block, G. J. Kapral, X. Wang, L. W. Murray, W. B. Arendall 3rd, J. Snoeyink, J. S. Richardson, and D. C. Richardson (2007) MolProbity: All-atom contacts and structure validation for proteins and nucleic acids. *Nucleic Acids Res*. 35: 375-383.
39. Dolinsky, T. J., J. E. Nielsen, J. A. McCammon, and N. A. Baker (2004) PDB2PQR: an automated pipeline for the setup of Poisson-Boltzmann electrostatics calculations. *Nucleic Acids Res*. 32: 665-667.
40. Baker, N. A., D. Sept, S. Joseph, M. J. Holst, and J. A. McCammon (2001) Electrostatics of nanosystems: Application to microtubules and the ribosome. *Proc. Natl. Acad. Sci. U. S. A*. 98: 10037-10041.
41. Schrödinger, L. L. C. (2010) The PyMOL molecular graphics system, version 1.3r1.
42. Bank, R. E. and M. Holst (2003) A new paradigm for parallel adaptive meshing algorithms. *SIAM Review* 45: 291-323.
43. Holst, M. (2001) Adaptive numerical treatment of elliptic systems on manifolds. *Adv. Comput. Math*. 15: 139-191.
44. Shaya, D., W. Zhao, M. Garron, Z. Xiao, Q. Cui, Z. Zhang, T. Sulea, R. Linhardt, and M. Cygler (2010) Catalytic mechanism of heparinase II investigated by site-directed mutagenesis and the crystal structure with its substrate *J. Biol. Chem*. 285: 20051-20061.
45. Frisch, M. J., G. W. Trucks, H. B. Schlegel, G. E. Scuseria, M. A. Robb, J. R. Cheeseman, V. G. Zakrzewski, J. A. Montgomery, R. E. Stratmann, J. C. Burant, S. Dapprich, J. M. Millam, A. D. Daniels, K. N. Kudin, M. C. Strain, O. Farkas, J. Tomasi, V. Barone, M. Cossi, R. Cammi, B. Mennucci, C. Pomelli, C. Adamo, S. Clifford, J. Ochterski, G. A. Petersson, P. Y. Ayala, Q. Cui, K. Morokuma, D. K. Malick, A. D. Rabuck, K. Raghavachari, J. B. Foresman, J. Cioslowski, J. V. Ortiz, B. B. Stefanov, G. Liu, A. Liashenko, P. Piskorz, I. Komaromi, R. Gomperts, R. L. Martin, D. J. Fox, T. Keith, M. A. Al-Laham, C. Y. Peng, A. Nanayakkara, C. Gonzalez, M. Challacombe, P. M.W. Gill, B. G. Johnson,W. Chen, M.W. Wong, J. L. Andres, M. Head-Gordon, E. S. Replogle, and J. A. Pople (1998) Gaussian 98 (Revision A.1) - Gaussian, Inc., Pittsburgh, PA.
46. Sanner, M. (1999) Python: A Programming Language for Software Integration and Development *J. Mol. Graphics Mod*. 17: 57-61.
47. Morris, G., R. Huey, W. Lindstrom, M. Sanner, R. Belew, D. Goodsell, and A. Olson (2009) AutoDock4 and AutoDockTools4: Automated docking with selective receptor flexibility *J. Comput. Chem*. 30: 2785-2791.
48. Patel, L. N., J. L. Zaro, and W. C. Shen (2007) Cell penetrating peptides: intracellular pathways and pharmaceutical perspectives. *Pharm. Res*. 24: 1977-1992.
49. Rothbard, J. B., T. C. Jessop, and P. A. Wender (2005) Adaptive translocation: the role of hydrogen bonding and membrane potential in the uptake of guanidinium-rich transporters into cells. *Adv. Drug. Deliv. Rev*. 57: 495-504.
50. Wender, P. A., D. J. Mitchell, K. Pattabiraman, E. T. Pelkey, L. Steinman, and J. B. Rothbard (2000) The design, synthesis, and evaluation of molecules that enable or enhance cellular uptake: Peptoid molecular transporters. *Proc. Natl. Acad. Sci. U. S. A*. 97: 13003-13008.
51. Alon, R., E. A. Bayer, and M. Wilchek (1990) Streptavidin contains an RYD sequence which mimics the RGD receptor domain of fibronectin. *Biochem. Biophys. Res. Commun*. 170: 1236-1241.
52. Alon, R., E. A. Bayer, and M. Wilchek (1992) Cell-adhesive properties of streptavidin are mediated by the exposure of an RGD-like RYD site. *Eur. J. Cell Biol*. 58: 271-279.
53. Alon, R., E. A. Bayer, and M. Wilchek (1993) Cell adhesion to streptavidin *via* RGD-dependent integrins. *Eur. J. Cell. Biol*. 60: 1-11.
54. Hollinshead, M., J. Sanderson, and D. J. Vaux (1997) Anti-biotin antibodies offer superior organelle-specific labeling of mitochondria over avidin or streptavidin. *J. Histochem. Cytochem*. 45: 1053-1057.
55. Rodriguez-Melendez, R. (2000) Importance of biotin metabolism. *Rev. Invest. Clin*. 52: 194-199.
56. Lehninger, A. L., D. L. Nelson, and M. M. Cox (2000) *Lehninger principles of biochemistry*. 3rd ed. Worth Publishers, NY, USA.
57. Vives, E. (2003) Cellular uptake of the Tat peptide: An endocytosis mechanism following ionic interactions. *J. Mol. Recognit*. 16: 265-271.